BIOCHEMISTRY

The deubiquitinase UCHL1 regulates cardiac hypertrophy by stabilizing epidermal growth factor receptor

Hai-Lian Bi[1], Xiao-Li Zhang[2], Yun-Long Zhang[1], Xin Xie[1], Yun-Long Xia[1], Jie Du[3], Hui-Hua Li[1,4]*

Pathological cardiac hypertrophy leads to heart failure (HF). The ubiquitin-proteasome system (UPS) plays a key role in maintaining protein homeostasis and cardiac function. However, research on the role of deubiquitinating enzymes (DUBs) in cardiac function is limited. Here, we observed that the deubiquitinase ubiquitin C-terminal hydrolase 1 (UCHL1) was significantly up-regulated in agonist-stimulated primary cardiomyocytes and in hypertrophic and failing hearts. Knockdown of UCHL1 in cardiomyocytes and mouse hearts significantly ameliorated cardiac hypertrophy induced by agonist or pressure overload. Conversely, overexpression of UCHL1 had the opposite effect in cardiomyocytes and rAAV9-UCHL1–treated mice. Mechanistically, UCHL1 bound, deubiquitinated, and stabilized epidermal growth factor receptor (EGFR) and activated its downstream mediators. Systemic administration of the UCHL1 inhibitor LDN-57444 significantly reversed cardiac hypertrophy and remodeling. These findings suggest that UCHL1 positively regulates cardiac hypertrophy by stabilizing EGFR and identify UCHL1 as a target for hypertrophic therapy.

INTRODUCTION

Sustained hypertrophic stress can evoke cardiac remodeling, frequently leading to heart failure (HF). Various pathologic stimuli including hypertension and pressure overload can elicit a hypertrophic response (*1*). Autocrine and paracrine signaling pathways involving angiotensin II (Ang II) also contribute to cardiomyocyte hypertrophy (*1*). Among the prohypertrophic pathways, the role of epidermal growth factor receptor (EGFR or ErbB1) as a positive regulator of cardiac hypertrophy has been clearly demonstrated (*2*). EGFR is a receptor tyrosine kinase of the ErbB family that activates multiple downstream signaling cascades, including the RAS/MEK (mitogen-activated protein kinase kinase)/ERK (extracellular signal–regulated kinase), PI3K (phosphatidylinositol 3-kinase)/AKT, and STAT (signal transducers and activators of transcription) pathways, subsequently regulating cell growth, proliferation, and survival (*3*). Increasing evidence has demonstrated that activation of EGFR is involved in blood pressure regulation, endothelial dysfunction, neointimal hyperplasia, atherogenesis, reactive oxygen species generation, and cardiac remodeling (*4*). Furthermore, EGFR stability, trafficking, and activation are mainly regulated by posttranslational modifications, including phosphorylation, acetylation, SUMOylation, and ubiquitination (*5*). However, the regulatory mechanisms of EGFR are not fully understood.

Posttranslational modification of cell proteins, including ubiquitination, is involved in the regulation of both membrane trafficking and protein degradation (*6*). Ubiquitination is a reversible process due to the presence of deubiquitinating enzymes (DUBs; also known as deubiquitinases) that can cleave ubiquitin from modified proteins. Ubiquitin C-terminal hydrolase 1 (UCHL1, also known as PARK5/PGP9.5), is a DUB responsible for removing ubiquitin or polyubiquitin from target proteins (*7*, *8*). It is highly dysregulated and plays critical roles in several disorders, including tumors, neurodegenerative diseases, and liver fibrosis (*8*, *9*). One study reported that UCHL1 influences skeletal muscle development and function. Deletion of UCHL1 in mice results in abnormal shuffling movement, hind-limb paralysis, and early death (*10*). Recently, UCHL1 expression was found to be highly up-regulated in cardiomyocytes after myocardial infarction and was associated with increased ubiquitin expression (*11*). However, little was known about the role of UCHL1 in regulating cardiac hypertrophy and remodeling.

In the present study, with loss- and gain-of-function approaches and inhibitor administration, we identified that UCHL1 acted as a positive regulator of cardiac hypertrophy by reducing EGFR ubiquitination and degradation. Administration of the UCHL1 inhibitor LDN-57444 confirmed the importance of UCHL1 for hypertrophy therapy. Together, these findings suggest that UCHL1 plays an important role in the pathogenesis of cardiac hypertrophy.

RESULTS

UCHL1 expression is up-regulated in hypertrophic and failing hearts

To determine the functions of DUBs in cardiac hypertrophy, we first performed microarray assays. Among the 53 deubiquitinase genes detected, UCHL1 mRNA expression was increased at day 1 (>1.2-fold), and the most up-regulated at days 3 and 7 in Ang II–infused hearts of wild-type (WT) mice compared with control (Fig. 1A and fig. S1A). Increased expression of UCHL1 mRNA was verified by real-time quantitative polymerase chain reaction (qPCR) analysis in Ang II–infused heart tissues (Fig. 1B). Moreover, the protein level of UCHL1 was significantly increased in Ang II– or phenylephrine (PE)–treated neonatal rat cardiomyocytes (NRCMs) in a time-dependent manner (Fig. 1, C and D). Similarly, the protein levels of UCHL1 were markedly up-regulated in the compensated hypertrophic hearts (at 2 weeks) and failing hearts (or decompensated stage at 4 weeks) in WT mice induced by transverse aortic constriction (TAC; Fig. 1E). Immunohistochemistry analysis further confirmed the increase in UCHL1 protein levels in the TAC-treated hearts

[1]Department of Cardiology, Institute of Cardiovascular Diseases, First Affiliated Hospital of Dalian Medical University, Dalian 11600, China. [2]Department of Medical Technology, Beijing Health Vocational College, Beijing 101101, China. [3]Beijing AnZhen Hospital the Key Laboratory of Remodeling-Related Cardiovascular Diseases, School of Basic Medical Sciences, Capital Medical University, Beijing 100029, China. [4]Department of Emergency Medicine, Beijing Key Laboratory of Cardiopulmonary Cerebral Resuscitation, Beijing Chaoyang Hospital, Capital Medical University, Beijing 100020, China.
*Corresponding author. Email: hhli1935@aliyun.com

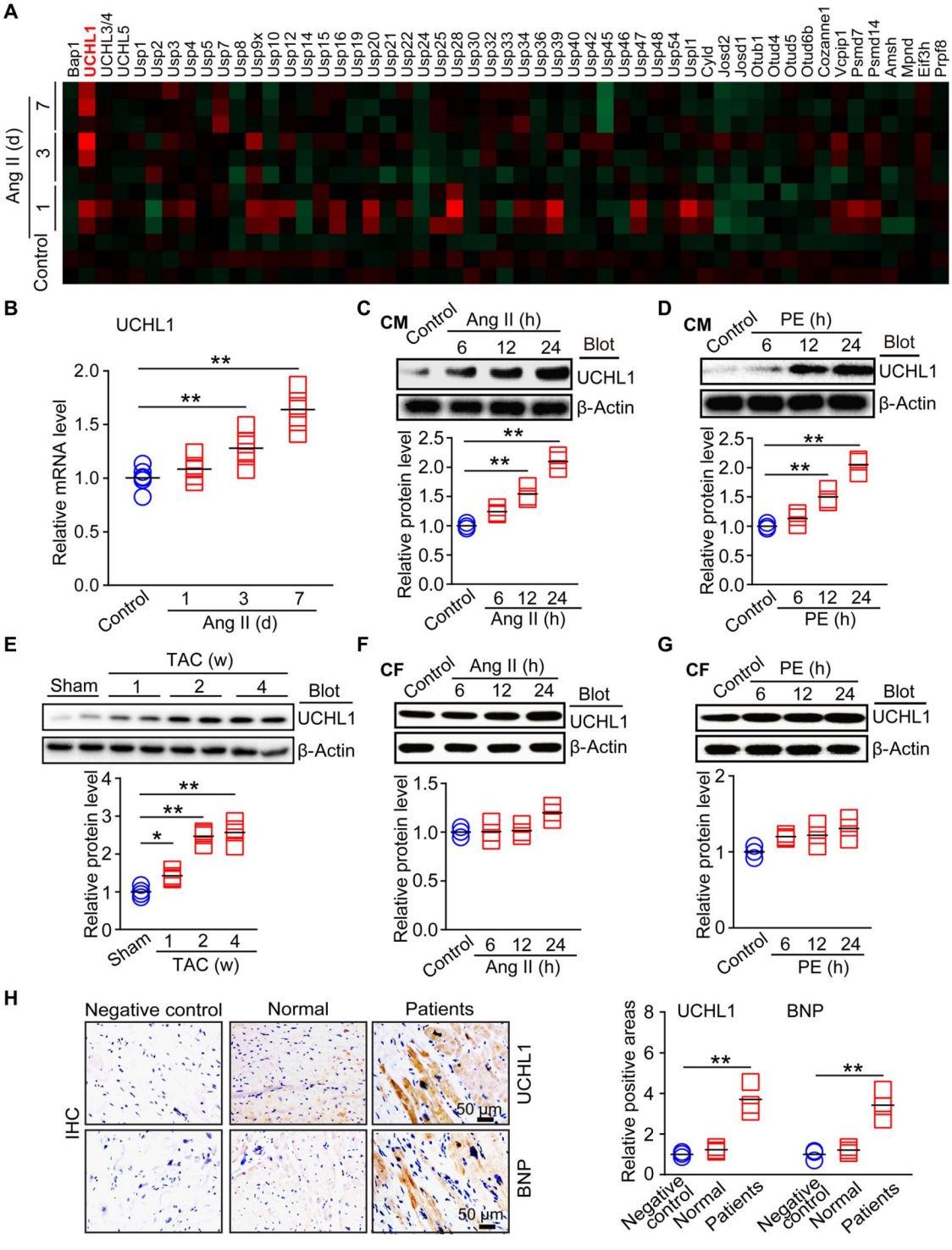

Fig. 1. UCHL1 is up-regulated in hypertrophic and failing hearts. (**A**) The cluster of deubiquitinase gene expression profiles in Ang II–infused mouse heart at days 1, 3, and 7 (d, day; $n = 3$). (**B**) qPCR analysis of UCHL1 mRNA expression in Ang II–infused mouse hearts ($n = 6$). (**C** and **D**) Representative immunoblotting analysis of UCHL1 protein level in NRCMs (CM) exposed to Ang II (100 nM) or PE (100 μM) at different time points (upper; h, hour). Quantification of the relative UCHL1 protein level (lower; $n = 3$). (**E**) Representative immunoblotting analysis of UCHL1 protein levels in the hearts after TAC at weeks 1, 2, and 4 (upper; w, week). Quantification of the relative UCHL1 protein level (lower; $n = 4$). (**F** and **G**) Representative immunoblotting analysis of UCHL1 protein level in NRCFs (CF) and treated as in (C) and (D). (**H**) Representative immunohistochemical (IHC) staining of UCHL1 (upper) and BNP (lower) proteins in the heart tissues from normal control and HF patients (left). Scale bars, 50 μm. Quantification of the relative UCHL1- and BNP-positive areas (right; $n = 3$). *n* represents the number of independent samples per group. $^*P < 0.05$; $^{**}P < 0.01$.

(fig. S1B). Meanwhile, the protein level of UCHL1 has no significant change in Ang II–treated neonatal rat cardiac fibroblasts (NRCFs; Fig. 1, F and G). Furthermore, immunohistochemistry results revealed that the expression levels of both UCHL1 and brain natriuretic peptide (BNP; a marker of HF) in human failing hearts were significantly higher than those in normal controls (Fig. 1H). Overall, these results suggest that increased UCHL1 expression may play a critical role in regulating cardiac hypertrophy and function.

Knockdown of UCHL1 reduces cardiac hypertrophy in vitro

To evaluate the effect of UCHL1 in the heart under a hypertrophic stimulus, we first examined whether UCHL1 exerts a pro- or anti-hypertrophic effect in vitro. NRCMs were infected with an adenovirus vector expressing small interfering RNA (siRNA) against UCHL1 (siRNA-UCHL1) or a scrambled control (siRNA-control). The level of endogenous UCHL1 protein was significantly decreased by approximately 50% (fig. S2A). Notably, knockdown of UCHL1 repressed the PE-induced increase in cardiomyocyte size and mRNA expression of hypertrophic markers including atrial natriuretic factor (ANF) and BNP (fig. S2, B and C). In contrast, we infected NRCMs with adenovirus overexpressing UCHL1 (Ad-UCHL1) or green fluorescent protein (Ad-GFP). Infection of NRCMs with Ad-UCHL1 increased the level of UCHL1 approximately 2.5-fold (fig. S2D) and markedly enhanced the PE-induced cardiomyocyte size and the mRNA levels of ANF and BNP compared with those in the Ad-GFP control (fig. S2, E and F). Moreover, we assessed a range of prohypertrophic pathways including EGFR, Ang II type 1 receptor (AT1R), insulin growth factor 1 receptor (IGF1R), glycoprotein130 (gp130), and their downstream signaling mediators. Knockdown of UCHL1 markedly reduced the protein levels of total EGFR and phosphorylated EGFR, AKT, and ERK1/2 (fig. S2G), with no effect on the EGFR mRNA level compared with the siRNA-controls after saline or PE stimulation (fig. S2H). However, knockdown of UCHL1 did not affect the other receptors, including AT1R, IGF1R, and gp130 after saline or PE treatment (fig. S2G). We also examined whether UCHL1 affected other members of the EGFR family and found that infection of NRCMs with siRNA-UCHL1 markedly reduced the EGFR protein level but did not significantly affect the protein levels of ErbB2, ErbB3, and ErbB4 compared with the siRNA-control (fig. S2I), indicating that UCHL1 selectively regulates EGFR stability. These results indicate that UCHL1 knockdown reduces cardiac hypertrophy, which may be related to the EGFR signaling pathway in vitro.

Heterozygous deletion of UCHL1 ameliorates pressure overload–induced cardiac hypertrophy and dysfunction

Given our positive in vitro findings (fig. S2), we evaluated the physiological consequences of UCHL1 deletion in vivo. Because of a progressive decrease in body weight (BW) and premature death of homozygous UCHL1 ($UCHL1^{-/-}$) mice at 12 weeks of age (*1*, *12*), we used heterozygous UCHL1 knockout ($UCHL1^{+/-}$) mice and WT ($UCHL1^{+/+}$) mice subjected to TAC for 2 weeks to generate a pressure overload–induced compensatory hypertrophy model. After 2 weeks of TAC, echocardiography showed compensatory cardiac hyperfunction as reflected by increased left ventricular (LV) ejection fraction (EF%) and fractional shortening (FS%) in TAC-operated $UCHL1^{+/+}$ mice compared with sham-operated animals, whereas this effect was markedly reversed in $UCHL1^{+/-}$ mice (fig. S3A). Moreover, TAC-operated $UCHL1^{+/+}$ mice developed cardiac hypertrophy as indicated by an increase in the ratios of HW (heart weight)/BW and HW/TL (tibia length), the cross-sectional area of myocytes, the extent of fibrosis, and the mRNA expression of ANF, BNP, β-myosin heavy chain (β-MHC), collagen I, and collagen III, whereas these changes were significantly abrogated in TAC-operated $UCHL1^{+/-}$ mice (fig. S3, B to G). There was no significant difference in these parameters between the two groups after sham operation (fig. S3, A to G). Consistent with the observations in cultured cardiomyocytes (fig. S2G), along with decreased UCHL1 protein levels, the levels of EGFR, phosphorylated AKT, and ERK1/2 were significantly reduced in $UCHL1^{+/-}$ hearts compared with $UCHL1^{+/+}$ hearts after TAC stress (fig. S3H). The protein levels of AT1R, IGF1R, and gp130 were not changed between the two groups after sham or TAC operation (fig. S3H). Thus, our in vivo data support that UCHL1 knockdown suppresses pressure overload–induced cardiac hypertrophy by selectively reducing EGFR signaling pathway in the heart in vivo.

To further assess whether heterozygous UCHL1 deletion prevents mice from developing HF, we extended the TAC operation imposed on $UCHL1^{+/+}$ and $UCHL1^{+/-}$ mice for 6 weeks. TAC resulted in a significant reduction in FS% and increases in LV internal diameter at the end of systole (LVIDs) and lung weight (LW)/TL ratio in $UCHL1^{+/+}$ mice compared with the sham groups, confirming the characteristics of HF. In contrast, this effect was markedly reversed in $UCHL1^{+/-}$ mice (Fig. 2A). Moreover, TAC induced a marked increase in the LV wall thickness, HW/BW and HW/TL ratios, cross-sectional area of myocytes, fibrotic area, and mRNA levels of ANF, BNP, β-MHC, collagen I, and collagen III in $UCHL1^{+/+}$ hearts, which were remarkably attenuated in $UCHL1^{+/-}$ mice (Fig. 2, B to F). Furthermore, as indicated by TUNEL (terminal deoxynucleotidyl transferase–mediated deoxyuridine triphosphate nick end labeling) staining, the number of cardiomyocytes undergoing apoptosis was significantly lower in $UCHL1^{+/-}$ hearts than in $UCHL1^{+/+}$ hearts after TAC (Fig. 2G). In addition, we observed a marked decrease in the total EGFR and phosphorylated EGFR, AKT, and ERK1/2 in the hearts of $UCHL1^{+/-}$ mice compared with $UCHL1^{+/+}$ mice after TAC (Fig. 2H). Collectively, these results demonstrate that knockdown of UCHL1 prevents the transition from compensated hypertrophy to HF.

Overexpressing UCHL1 in cardiomyocytes accelerates pressure overload–induced cardiac hypertrophy

To further confirm whether UCHL1 overexpression promotes cardiac hypertrophy in vivo, we generated the cardiotropic recombinant adeno-associated virus serotype 9 (rAAV9) expressing Flag-tagged UCHL1 (fig. S4A), which was delivered into WT mice via tail vein injection. The efficiency of UCHL1 gene transfer in the heart was determined by fluorescence microscopy for Flag tag and GFP protein (fig. S4B). WT mice were then subjected to sham or TAC operation for an additional 4 weeks (Fig. 3A). Immunoblotting showed that rAAV9-UCHL1 injection increased expression by 1.7- or 2.2-fold after sham or TAC, respectively, after injection (Fig. 3B). The expression of UCHL1 in the heart was also confirmed by immunoblotting with anti-Flag antibody (fig. S4C). The death rates of mice administered 5×10^{11} vg of rAAV9-UCHL1 were significantly higher than those of control mice administered rAAV9-GFP after 4 weeks of TAC (fig. S4D). Echocardiography revealed that injection of rAAV9-UCHL1 resulted in more severe cardiac dysfunction reflected by decreased FS% and increased LVIDs and LW/TL ratio compared to rAAV9-GFP controls (Fig. 3C). Furthermore, rAAV9-UCHL1–injected

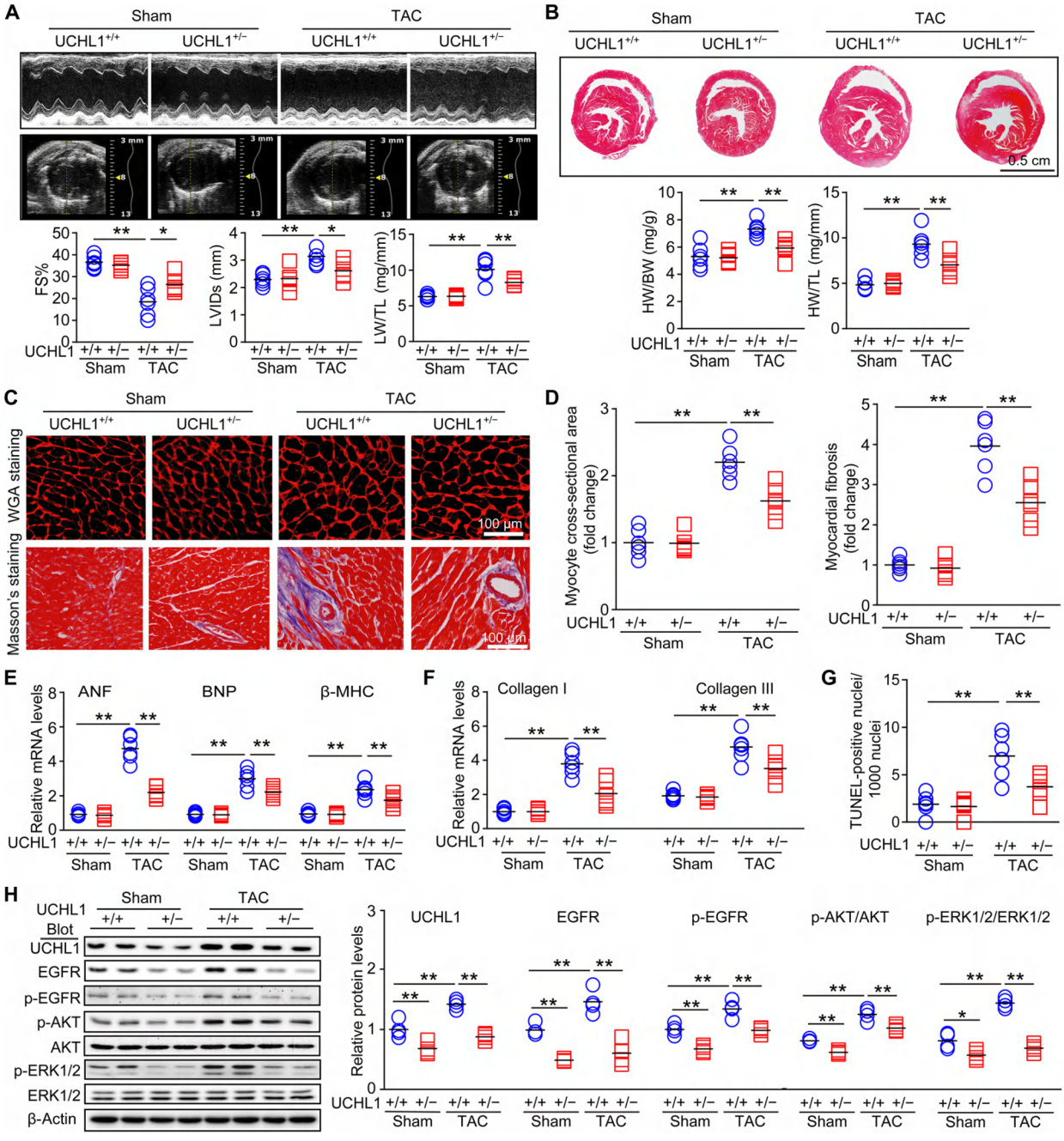

Fig. 2. UCHL1 knockdown ameliorates HF in mice after 6 weeks of TAC operation. WT (UCHL1$^{+/+}$) and heterozygous UCHL1 knockout (UCHL1$^{+/-}$) mice were subjected to sham or TAC operation for 6 weeks. (**A**) Representative M-mode and B-mode echocardiography of left ventricular chamber (upper). Measurement of FS%, LVIDs, and LW to TL ($n = 6$ mice per group) (**B**) Representative heart sections examined by hematoxylin and eosin (H&E) staining (upper). Scale bar, 0.5 cm. HW/BW and HW/TL ratios (lower; $n = 6$). (**C**) TRITC-labeled wheat germ agglutinin (WGA) staining of myocyte hypertrophy (upper). Masson's trichrome staining of myocardial fibrosis (lower). Scale bars, 100 μm. (**D**) Quantification of the relative myocyte cross-sectional area [200 cells counted per heart (left); $n = 6$ mice per group] and the relative fibrotic area (right; $n = 6$). (**E**) qPCR analysis of ANF, BNP, and β-MHC mRNA expression ($n = 6$ mice per group). (**F**) qPCR analysis of collagen I and III mRNA expression ($n = 6$ mice per group). (**G**) TUNEL assay of cardiac myocyte apoptosis in the hearts. Quantification of TUNEL-positive nuclei ($n = 6$ mice per group). (**H**) Representative immunoblotting analysis and quantification of UCHL1, EGFR, p-EGFR, AKT, p-AKT, ERK1/2, and p-ERK1/2 protein levels in the heart tissues ($n = 4$ mice per group). β-Actin as an internal control. *n* represents the number of independent samples per group. *$P < 0.05$; **$P < 0.01$.

mice showed a significant increase in heart size, LV dilation, HW/BW and HW/TL ratios, cross-sectional area of myocytes, collagen deposition, and mRNA expression levels of BNP, β-MHC, collagen I, and collagen III compared with the rAAV9-GFP control after TAC (Fig. 3, C to 3H). The number of TUNEL-positive nuclei in the rAAV9-UCHL1–injected mice was also significantly higher than that in rAAV9-GFP–injected mice after TAC (Fig. 3I). In parallel with the increased expression of UCHL1, the levels of EGFR protein

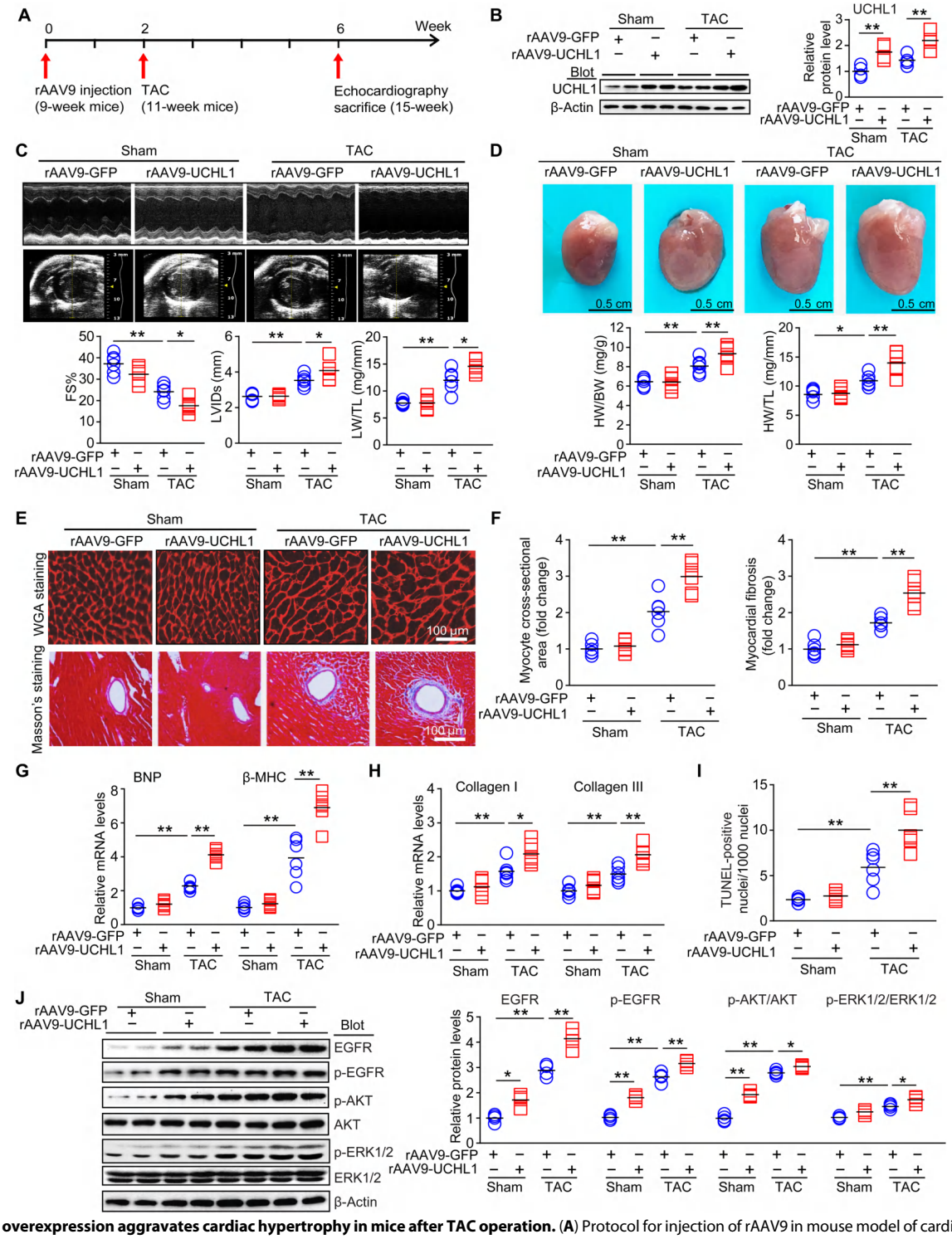

Fig. 3. UCHL1 overexpression aggravates cardiac hypertrophy in mice after TAC operation. (**A**) Protocol for injection of rAAV9 in mouse model of cardiac hypertrophy and remodeling. WT mice were injected with rAAV9-GFP or rAAV9-UCHL1 for 2 weeks and then subjected to sham or TAC for additional 4 weeks. (**B**) Representative immunoblotting analysis (left) and quantification of UCHL1 in the hearts (right; $n = 4$ mice per group). (**C**) Representative M-mode and B-mode echocardiography of LV chamber (upper). Measurement of FS%, LVIDs, and LW/TL (lower; $n = 6$ mice per group). (**D**) Representative heart sizes from each group (upper). Scale bars, 0.5 cm. The ratios of HW/BW and HW/TL (lower; $n = 6$ per group). (**E**) Histological examination of cardiac hypertrophy by TRITC-WGA staining (upper). Myocardial fibrosis detected by Masson's trichrome staining (lower). Scale bars, 100 μm. (**F**) Quantification of the relative myocyte cross-sectional area (200 cells counted per heart, lower; $n = 6$) and the relative fibrosis area (lower; $n = 6$). (**G**) qPCR analysis of BNP and β-MHC mRNA levels in the hearts. The data are normalized to the GAPDH expression ($n = 6$ per group). (**H**) qPCR analysis of collagen I and III mRNA levels. The data are normalized to the GAPDH expression ($n = 6$ per group). (**I**) Quantification of TUNEL-positive nuclei in the hearts ($n = 6$ per group). (**J**) Representative immunoblotting analysis and quantification of EGFR, p-EGFR, AKT, p-AKT, ERK1/2, and p-ERK1/2 protein levels in the hearts ($n = 4$ mice per group). β-Actin as an internal control. *n* represents the number of independent samples per group. $^*P < 0.05$; $^{**}P < 0.01$.

and phosphorylated EGFR, AKT, and ERK1/2 in the myocardium were significantly increased in rAAV9-UCHL1–injected mice compared with rAAV9-GFP controls after TAC (Fig. 3J). In addition, 4 weeks after sham surgery, injection of mice with rAAV9-UCHL1 markedly increased the protein levels of total EGFR and phosphorylated EGFR and AKT (Fig. 3J) but did not significantly accelerate cardiac dysfunction, hypertrophy, and fibrosis compared with the rAAV9-GFP control (Fig. 3, C to G), suggesting that short-term overexpression of UCHL1 had no effect on the heart. Overall, these results suggest that cardiac-specific expression of UCHL1 aggravates cardiac hypertrophy and may be associated with EGFR stability.

UCHL1 interacts with EGFR

To investigate how UCHL1 regulates EGFR stability, we performed a coimmunoprecipitation (Co-IP) assay to evaluate whether UCHL1 associates with EGFR. We found that EGFR was efficiently precipitated by an antibody against UCHL1, but not by control immunoglobulin G (IgG) in NRCMs. Unlike EGFR, UCHL1 did not interact with gp130, IGF1R, or AT1R (Fig. 4A). This interaction of UCHL1 with EGFR was enhanced by PE treatment (Fig. 4B). Moreover, reverse Co-IP further confirmed that UCHL1 was markedly precipitated by an antibody against EGFR in NRCMs (Fig. 4C). A Co-IP assay was performed with epitope-tagged proteins in human embryonic kidney (HEK) 293 T cells. Myc-tagged UCHL1 also highly coprecipitated with Flag-tagged EGFR (Fig. 4D). These results suggest that UCHL1 interacts with EGFR in cardiomyocytes.

To determine the sequences in UCHL1 that may mediate the interaction with EGFR, we used epitope-tagged proteins (full-length UCHL1 and a series of UCHL1 deletion mutants) for their ability to bind full-length Flag-tagged EGFR expressed in HEK293T cells. Because GFP-tagged UCHL1 is approximately 50 kDa and therefore difficult to distinguish from IgG, we used Myc-tagged UCHL1 rather than GFP-tagged UCHL1. Co-IP assays with anti-Myc antibody or anti-GFP antibody revealed that the N-terminal peptide representing amino acid residues 1 to 175 was the most strongly bound to EGFR and that deletion of amino acid 90 to 175 markedly reduced the interaction of UCHL1 with EGFR. However, the deletion of the N-terminal truncation (Δ1 to 90 amino acids) could not bind to EGFR, indicating that the region of amino acid residues 1 to 90 of UCHL1 is required for EGFR binding and that the region of 90 to 175 amino acids also plays a role in mediating the interaction (fig. S4A). These data are summarized in fig. S4B. To further identify the regions in EGFR required for the interaction with UCHL1, a series of truncations of Flag-tagged EGFR was used in Co-IP assays with Myc-tagged UCHL1 expressed in HEK293T. The intracellular domain (669 to 1209 amino acids) of EGFR was necessary for the interaction between EGFR and UCHL1 (fig. S4, C and D).

UCHL1 inhibits EGFR ubiquitination and degradation

UCHL1 is a DUB; we therefore studied whether it regulates EGFR ubiquitination and degradation in cardiomyocytes. NRCMs were infected with siRNA-UCHL1 or siRNA-control, and immunoprecipitation was performed with an anti-EGFR antibody. Knockdown of UCHL1 significantly enhanced EGFR ubiquitination but decreased the EGFR level compared with the siRNA-control (Fig. 4E). To validate the effect of UCHL1 on EGFR ubiquitination, HEK293T cells were cotransfected with plasmids GFP-tagged EGFR, Myc-tagged UCHL1, either WT or a catalytically inactive mutant (C90S), which is critical for both the hydrolase and ligase activity of UCHL1 (*13*, *14*), and Flag-tagged ubiquitin. As expected, overexpression of UCHL1 (WT) significantly abrogated EGFR ubiquitination and increased EGFR levels, whereas this effect was reversed by UCHL1 (C90S; Fig. 4F). Moreover, NRCMs were infected with indicated siRNAs and then treated with cycloheximide (CHX; an inhibitor of protein synthesis). Knockdown of UCHL1 significantly decreased the half-life of EGFR protein compared with the control group (Fig. 4G), whereas its half-life was markedly increased in Ad-UCHL1–infected NRCMs compared with the Ad-GFP control (Fig. 4H). In addition, the effect of endogenous UCHL1 on EGFR ubiquitination was detected in $UCHL1^{+/-}$ mice or WT mice injected with rAAV9-UCHL1. We found that the ubiquitination and degradation of EGFR were significantly increased in $UCHL1^{+/-}$ hearts compared with $UCHL1^{+/+}$ control mice (fig. S5E), but markedly reduced in rAAV9-UCHL1–injected mice compared with the rAAV9-GFP control after sham or TAC treatment (fig. S5F). Together, these results indicate that EGFR is a substrate for UCHL1 in cardiomyocytes and hypertrophic hearts.

It is well known that epidermal growth factor (EGF) is an EGFR ligand that binds to and stimulates EGFR activation and subsequent degradation. An immunoprecipitation assay was performed revealing that UCHL1 bound to EGFR, which was not significantly influenced by EGF treatment in NRCMs (fig. S5G). In addition, knockdown of UCHL1 increased EGFR polyubiquitination and decreased the EGFR level with or without EGF stimulation (fig. S5H). These data suggest that UCHL1 also regulates the level of EGFR ubiquitination independent of EGF.

UCHL1 accelerates cardiac hypertrophy by increasing EGFR level

As our preceding data showed that UCHL1 interacted with and stabilized EGFR (Figs. 2 to 4), we next tested whether UCHL1 promotes cardiac hypertrophy by selectively targeting EGFR and the downstream signaling pathway. First, NRCMs were infected with Ad-UCHL1 or empty vector GFP (Ad-GFP) together with siRNA-EGFR or siRNA-control. As expected, overexpression of UCHL1 significantly enhanced cardiomyocyte size, the mRNA level of ANF, and the protein levels of EGFR, and phosphorylated EGFR, AKT, and EKR1/2 compared with coinfection with Ad-GFP and siRNA-control after PE stimulation; moreover, this effect was markedly attenuated by coinfection with Ad-GFP or Ad-UCHL1 and siRNA-EGFR (fig. S6, A to C). There was no significant difference in cardiomyocyte size and the mRNA level of ANF between the groups treated with saline, although the protein levels of EGFR, p-EGFR, p-AKT, and p-ERK1/2 were markedly up-regulated in Ad-UCHL1–infected cardiomyocytes compared with the Ad-GFP–injected cells (fig. S6, A to C; lane 2 versus 1). These in vitro data suggest that UCHL1 mediates PE-induced cardiomyocyte hypertrophy by increasing EGFR signaling.

To further examine whether overexpression of UCHL1 in cardiomyocytes accelerates hypertrophy and dysfunction by influencing the stability of EGFR in vivo, we generated cardiomyocyte-specific UCHL1-overexpressing and EGFR knockdown mice by injection with rAAV9-UCHL1 and rAAV9-siEGFR or their corresponding controls because EGFR full-knockout mice exhibit embryonic lethality (*15*). Consistent with the results in Fig. 3, we found that overexpression of UCHL1 caused cardiac dysfunction (decreased EF% and FS%), LV chamber hypertrophy (increased HW/BW and HW/TL ratios, cross-sectional area of myocytes, and mRNA expression levels of ANF, BNP, and β-MHC), and myocardial fibrosis (increased collagen deposition and mRNA expression levels of collagen I and collagen

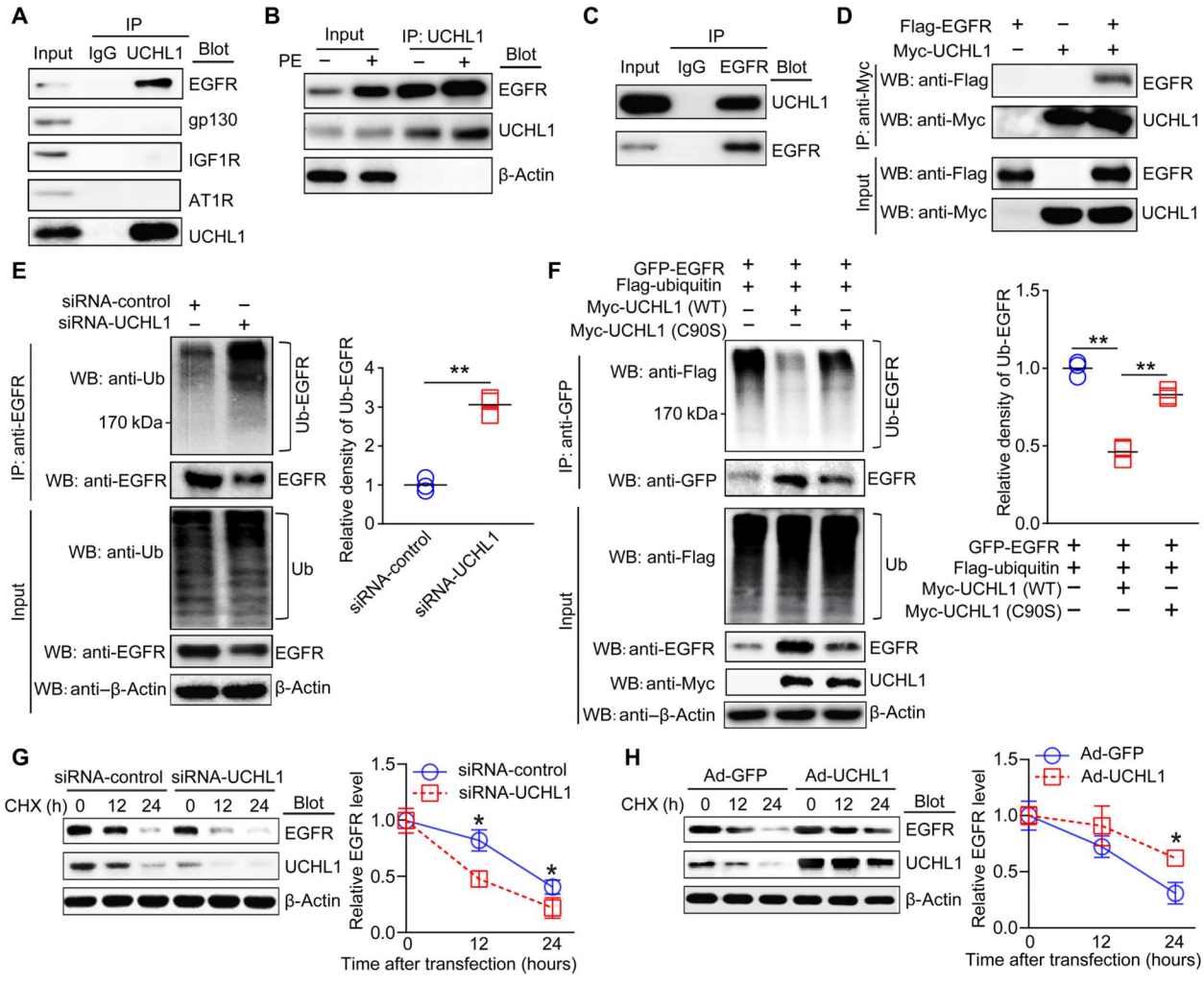

Fig. 4. UCHL1 interacts with EGFR and inhibits its degradation. (**A**) Endogenous protein interactions were examined in cardiomyocyte lysates immunoprecipitated (IP) with anti-rabbit IgG or anti-UCHL1 antibody, and analyzed by Western blot (WB) with antibodies to detect EGFR, gp130, IGF1R, AT1R, and UCHL1 ($n = 3$). (**B**) Lysates from NRCMs stimulated with PE (100 μM) for 24 hours. Equal amounts of protein lysates were immunoprecipitated with anti-UCHL1 antibody and analyzed by WB with the indicated antibodies ($n = 3$). (**C**) Endogenous protein interactions were further confirmed in cardiomyocyte lysates immunoprecipitated with anti-rabbit IgG or anti-EGFR, and analyzed by WB with the indicated antibodies ($n = 3$). (**D**) Exogenous protein interactions were demonstrated in HEK293T. Lysates from HEK293T cells transfected with Myc-tagged UCHL1 and Flag-tagged EGFR plasmids were immunoprecipitated with anti-Myc followed by WB with anti-Flag (EGFR) and anti-Myc (UCHL1) ($n = 3$). (**E**) Lysates from NRCMs infected with adenovirus siRNA-control or siRNA-UCHL1 followed by treatment with MG132 for 6 hours before harvest and were immunoprecipitated and detected with indicated antibodies (left). Quantification of the relative ubiquitin-EGFR (Ub-EGFR) level (right; $n = 3$). (**F**) Lysates from HEK293T cells transfected with Flag-tagged ubiquitin (Ub) and GFP-tagged EGFR together with Myc-tagged UCHL1 (WT) or Myc-tagged UCHL1 mutant (C90S) followed by treatment with MG132 for 6 hours before harvest were immunoprecipitated with anti-GFP antibody followed by WB with anti-Flag (Ub) and anti-GFP (EGFR) (left). Quantification of the relative Ub-EGFR level (right; $n = 3$). (**G** and **H**) NRCMs were infected with siRNA-control, siRNA-UCHL1, Ad-GFP, or Ad-UCHL1, and then treated with CHX (10 μM) for the indicated time periods. Representative Western blot analysis of UCHL1 and EGFR protein levels for each group (left), and quantification of EGFR level (right; $n = 3$). β-Actin as an internal control, and n represents the number of independent samples per group. $^*P < 0.05$; $^{**}P < 0.01$.

III), and enhanced the protein levels of total EGFR and phosphorylation of EGFR, AKT, and EKR1/2 compared with the rAAV9-GFP control after TAC (Fig. 5, A to G; lane 2 versus 1), whereas these effects were remarkably reduced in mice coinjected with rAAV9-GFP and rAAV9-siEGFR or coinjected with rAAV9-UCHL1 and rAAV9-siEGFR (Fig. 5, A to G; lane 4 versus 2, and lane 3 versus 1). There were no significant differences in the pathological changes between the groups in sham treatment, although the protein levels of EGFR, p-EGFR, p-AKT, and p-ERK1/2 were highly increased in rAAV9-UCHL1–infected mice compared with those in the rAAV9-GFP–injected animals (fig. S7; lane 2 versus 1). Together, these results indicate that UCHL1 mediates cardiac hypertrophy and remodeling through deubiquitination and stabilization of EGFR in vivo.

Administration of LDN-57444 reverses cardiac hypertrophy

To further assess whether inhibition of UCHL1 reverses the pre-established cardiac hypertrophic remodeling, we used the small-molecule UCHL1 inhibitor LDN-57444 (LDN) to treat mice, which is a specific inhibitor of UCHL1 (*13*, *16*, *17*). WT mice were subjected

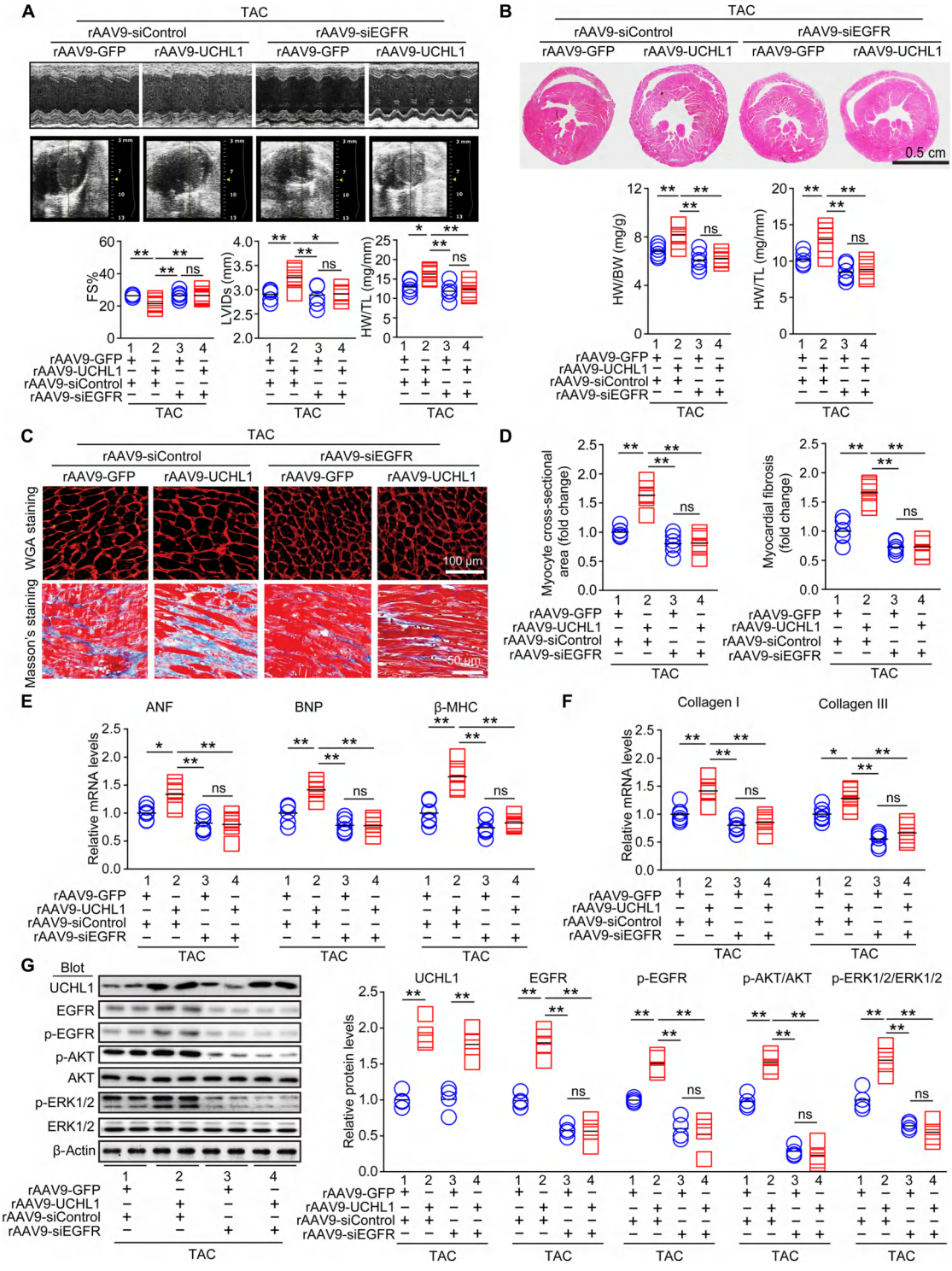

Fig. 5. The stabilization of EGFR is critical for UCHL1-mediated cardiac hypertrophy and dysfunction in vivo. WT mice were injected with rAAV9-GFP or rAAV9-UCHL1 and rAAV9-siControl or rAAV9-siEGFR as indicated for 2 weeks, and then subjected to TAC for an additional 4 weeks. (**A**) Representative M-mode and B-mode echocardiography of LV chamber (upper). Measurement of FS%, LVIDs, and LW/TL ($n = 6$ mice per group). (**B**) Representative images of H&E staining of the heart sections (upper). Scale bar, 0.5 cm. The ratios of HW/BW and HW/TL (lower) ($n = 6$ per group). (**C**) Histological examination of cardiac hypertrophy by TRITC-WGA staining (upper). Myocardial fibrosis detected by Masson's trichrome staining (lower). Scale bars, 100 or 50 μm as indicated. (**D**) Quantification of the relative myocyte cross-sectional area [200 cells counted per heart (left); $n = 6$ per group) and the relative fibrosis area (right; $n = 6$). (**E**) qPCR analysis of ANF, BNP, and β-MHC mRNA levels in the hearts. The data are normalized to the GAPDH expression ($n = 6$ per group). (**F**) qPCR analysis of collagen I and III mRNA levels. The data are normalized to the GAPDH expression ($n = 6$ per group). (**G**) Representative immunoblotting analysis and quantification of UCHL1, EGFR, p-EGFR, AKT, p-AKT, ERK1/2, and p-ERK1/2 protein levels in the hearts ($n = 4$ mice per group). β-Actin as an internal control. *n* represents the number of independent samples per group. $^*P < 0.05$; $^{**}P < 0.01$.

to TAC for 2 weeks and then randomized to be administered vehicle only or LDN for an additional 2 weeks. Four weeks after TAC, a significant reversal in cardiac contractile dysfunction, hypertrophy, myocardial fibrosis, and TUNEL-positive cell apoptosis was observed in LDN-treated TAC mice compared with TAC mice alone (Fig. 6, A to G, and table S1), indicating that LDN reversed the transition from

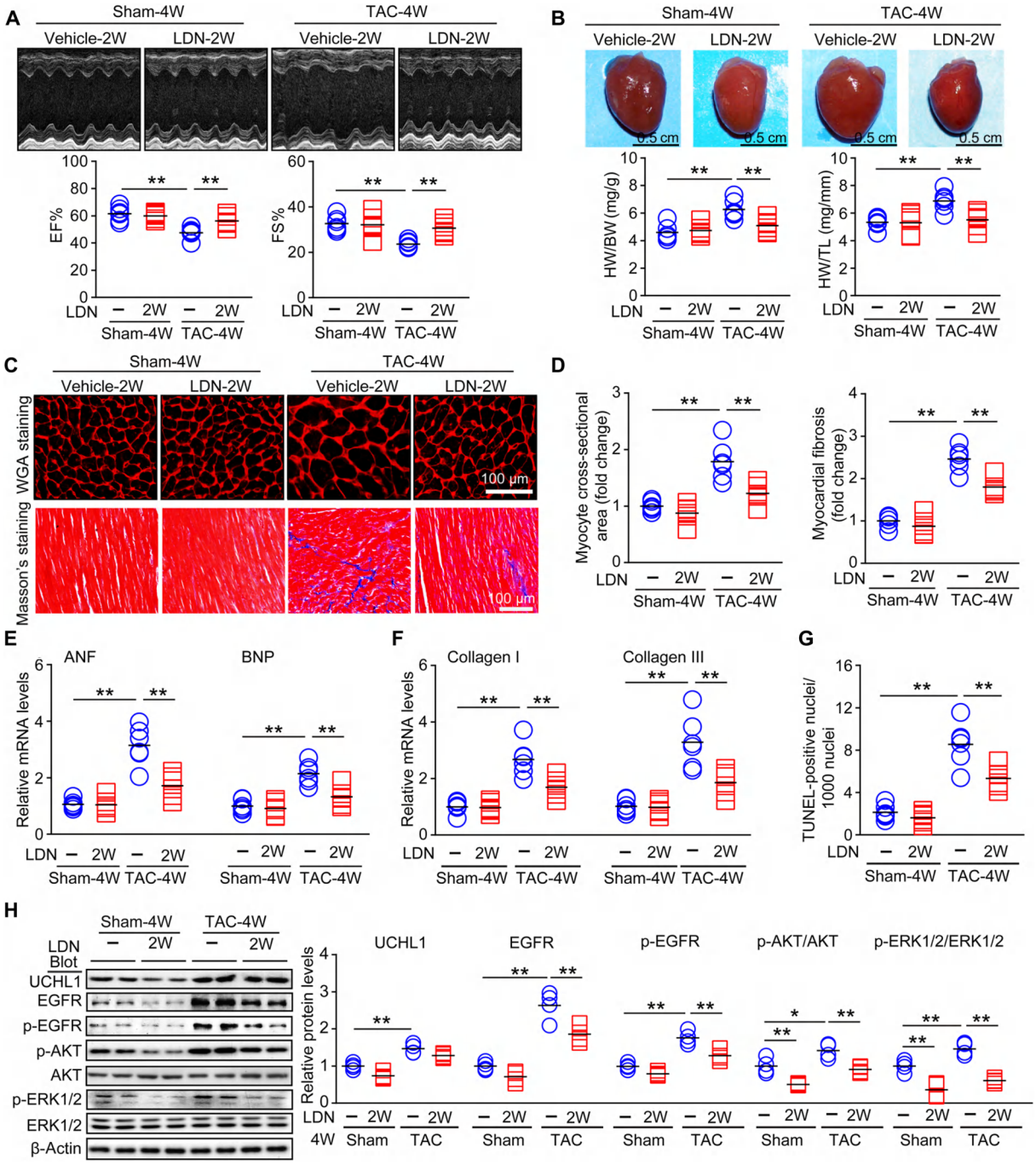

Fig. 6. UCHL1 inhibitor reverses preestablished cardiac hypertrophy after 4 weeks of TAC. WT mice were subjected to sham or TAC operation for 2 weeks and then treated with LDN for additional 2 weeks. (**A**) Representative M-mode echocardiography of LV chamber (upper), and measurement of EF% and FS% (lower; $n = 6$). (**B**) Representative heart sizes from each group (upper). Scale bars, 0.5 cm. HW/BW and HW/TL ratios ($n = 6$ mice per group; lower). (**C**) Representative TRITC-WGA staining of the heart sections (upper). Masson's trichrome staining of myocardial fibrosis (lower). Scale bars, 100 μm. (**D**) Quantification of the relative myocyte cross-sectional area (200 cells counted per heart; left) and the relative fibrosis area (right; $n = 6$). (**E**) qPCR analysis of ANF and BNP mRNA levels in the hearts. The data are normalized to the GAPDH expression ($n = 6$ per group). (**F**) qPCR analysis of collagen I and III mRNA levels. The data are normalized to the GAPDH expression ($n = 6$ per group). (**G**) Quantification of TUNEL-positive nuclei ($n = 6$ mice per group). (**H**) Representative immunoblotting analysis and quantification of the protein levels of UCHL1, EGFR, p-EGFR, AKT, p-AKT, ERK1/2, and p-ERK1/2 in the hearts ($n = 4$ mice per group). β-Actin as an internal control. *n* represents the number of independent samples per group. *$P < 0.05$; **$P < 0.01$.

compensatory hypertrophy to cardiac remodeling. No significant difference was observed between the two groups after sham operation for these variables (Fig. 6, A to G). Moreover, the total EGFR and phosphorylated EGFR, AKT, and ERK1/2 levels were markedly reduced in LDN-treated mice after TAC or sham operation (Fig. 6H). These results indicate that UCHL1 is a good therapeutic target for treating cardiac hypertrophy and remodeling.

DISCUSSION

In this study, the use of loss- and gain-of-function approaches revealed a novel role for UCHL1 in regulating cardiac hypertrophy and dysfunction. UCHL1 positively regulates cardiac hypertrophy by attenuating EGFR ubiquitination and degradation. Moreover, cardiac hypertrophy and remodeling can be reversed by administration of the UCHL1 inhibitor LDN in mice. Therefore, this study identifies UCHL1 as a potential therapeutic target for treating hypertrophic diseases.

Increasing evidence demonstrates that UCHL1 is a deubiquitinase with important roles in regulating cancer, neurodegenerative diseases, and the inflammatory response by abrogating the ubiquitination of multiple proteins, including c-Jun activation domain-binding protein-1 (JAB1), $p27^{Kip1}$, hypoxia-inducible factor-1α (HIF-1α), p53, inhibitor of nuclear factor κB-α (IκB-α), and beta-site amyloid precursor protein cleaving enzyme 1 (BACE1) (*18*–*20*). Among them, BACE1 expression is increased in human HF (*21*). p53 aggravates cardiac dysfunction, remodeling, and apoptosis by partially inhibiting HIF1α and vascular endothelial growth factor (*22*). $p27^{Kip1}$ down-regulation is positively associated with hypertension (*23*). Stabilization of IκB-α inhibits pressure overload–induced nuclear factor κB (NF-κB) activation and hypertrophy (*24*). However, it is unclear whether these substrates are involved in the hypertrophic effects of UCHL1. To test the effect of UCHL1 in the heart, we detected UCHL1 expression and found that it was markedly up-regulated in agonist-stimulated cardiomyocytes and in hypertrophic and failing hearts (Fig. 1), suggesting a role for UCHL1 in the development of pathological cardiac hypertrophy. Our data clearly showed that UCHL1 knockdown significantly ameliorated cardiac hypertrophy and dysfunction, whereas increased UCHL1 expression aggravated these effects in vitro and in vivo (Figs. 2 and 3, and fig. S3). Previous studies reported that UCHL1 mRNA expression was up-regulated in isoproterenol-induced pathological hypertrophy, but unchanged in exercise-induced cardiac hypertrophy (*25*), suggesting that UCHL1 may not be involved in the development of physiological hypertrophy. In addition to UCHL1, the expression levels of 13 other genes were also increased (>1.2-fold) compared with control at day 1, but not at day 3 or day 7 of Ang II infusion (fig. S1A). Among them, several DUBs have been reported to participate in cardiac diseases. For example, ubiquitin carboxyl-terminal hydrolase 20 (USP20) knockout reduces β1-adrenergic receptor (β1AR)–induced cardiac contractility and relaxation (*26*). USP7 is a p53 deubiquitinating protein that promotes doxorubicin-induced cardiotoxicity in aged hearts (*27*). Moreover, cylindromatosis (CYLD) knockout attenuates pressure overload–induced cardiac oxidative stress, remodeling, and dysfunction through up-regulation of Nrf2-mediated antioxidant effect (*28*). Collectively, these results demonstrate a prohypertrophic role of UCHL1 in the heart after pathological stimuli. However, the molecular mechanism by which Ang II, PE, or TAC up-regulates UCHL1 expression remains to be determined.

It has been widely reported that posttranslational modifications play a critical role in regulating EGFR stability, activation, and trafficking (*5*, *29*), possibly influencing the effect of EGFR in the development of cardiac remodeling. Among them, ubiquitination induced by different E3s promotes the degradation of EGFR, leading to inhibition of its downstream signals (*30*, *31*). In contrast, some DUBs (AMSH, UBPY/Usp8, USP18, Cezanne-1, and USP2a) appear to be specific for the deubiquitination of EGFR in different cell types (*32*, *33*); however, the expression of these DUBs was not significantly changed at the mRNA expression level at different time points after Ang II infusion (Fig. 1A), indicating that they were not involved in regulating EGFR in cardiomyocytes. Fortunately, our findings are consistent with the results of yeast two-hybrid assay, which suggested that EGFR is related to UCHL1 (*5*). Here, we provided convincing evidence that UCHL1 was stably associated with EGFR (Fig. 4E) and reduced the ubiquitination of EGFR, leading to inhibition of EGFR degradation in both NRCMs and heart tissues (Fig. 4, E to H, and fig. S5, E and F). Furthermore, knockdown of EGFR abolished the UCHL1 overexpression–mediated induction of cardiac hypertrophy in vitro and in vivo (Fig. 5 and fig. S6), suggesting that EGFR stability and activity are essential for the beneficial effect of UCHL1 on cardiomyocyte hypertrophy. These results indicate that UCHL1 modulates cardiac hypertrophy and dysfunction likely by targeting EGFR stability.

Several mechanisms regulate the expression of EGFR in response to various stimuli. In addition to the transcriptional regulation of EGFR gene expression by Y-box binding protein-1, β-catenin, and Stat5b (*34*–*36*), activation of EGFR can be stimulated by two pathways: ligand-dependent and ligand-independent signaling. EGF is a high-affinity ligand of EGFR. It is widely accepted that EGF binds to the extracellular domain of EGFR to induce the dimerization of EGFR and the activation of its kinase (*37*). In this study, we found that EGF stimulation did not alter the interaction between UCHL1 and EGFR. Moreover, the effect of UCHL1 on the ubiquitination of EGFR did not involve exchange by EGF stimulation (fig. S5, C and D), suggesting that UCHL1 regulates EGFR stability and activation in a ligand-independent manner. EGFR can be transactivated by a growing number of different pathways, including G protein–coupled receptors and other receptors (*38*). Several studies suggest that pressure overload can induce EGFR transactivation during cardiac hypertrophy. Consistent with these findings, our results revealed that multiple hypertrophic stimuli increased EGFR protein level and activation (Figs. 2H and 3J, and fig. S2G), indicating that EGFR transactivation plays an important role in this disease.

Another important finding was that the administration of LDN was sufficient and effective to reverse cardiac hypertrophy and dysfunction after hypertrophic stimuli (Fig. 6). LDN has been identified as a UCHL1-specific inhibitor and used for the treatment of various disorders in animals and cells, including liver fibrosis, neurodegenerative diseases, and tumor metastases (*7*, *16*, *17*). Although UCHL1-specific inhibitors have been developed, no clinically approved UCHL1 inhibitors are currently available. Our data suggested that moderate LDN could be of clinical interest given its ability to improve cardiac hypertrophy and dysfunction without cardiotoxicity. Together, these data highlight the importance of the UCHL1-mediated posttranslational mechanism of EGFR in cardiomyocytes in vitro and in vivo. Moreover, the inhibition of UCHL1 as a therapeutic strategy for hypertrophic diseases should be further investigated.

MATERIALS AND METHODS

Animals

All experiments were approved by the Animal Care and Use Committee of Dalian Medical University and performed in accordance with the U.S. National Institutes of Health (NIH) *Guide for the Care and Use of Laboratory Animals* (publication no. 85-23, 1996). C57BL/6J WT and Uchl1$^{gad\text{-}2J}$ (UCHL1$^{+/-}$) mice were purchased from the Jackson laboratory (Bar Harbor, ME, USA). All mice were previously backcrossed over 10 generations to the C57BL/6 background. For all in vivo studies, age- and sex-matched WT and UCHL1$^{+/-}$ mice were used with at least five mice per genotype.

Cell lines and plasmids

HEK293T cells were obtained from the American Type Culture Collection (ATCC; Manassas, VA, USA). The plasmids pCMV2-Flag vector, pCMV2-Flag-hUCHL1, pcDNA3.1-Myc-hUCHL1 (WT), and pcDNA3.1-Myc-hUCHL1 (mutant C90S) were generously provided by K.-J. Lee (Ewha Womans University, Seoul, Republic of Korea) (*39*). The plasmids pcDNA3.1-GFP-hUCHL1 mutants (ΔN,ΔC, and Δ90 to 175), pCMV10-Flag-hEGFR WT, and pCMV10-Flag-hEGFR mutants (1 to 646, 1 to 668, and 669 to 1209) were constructed by Beijing SyngenTech Co., Ltd. (Peking, China). The plasmid pCMV3-GFPSpark-rat EGFR was purchased from Sino Biological Inc. (Peking, China).

Cell culture and adenoviral infection

NRCMs and NRCFs were enzymatically isolated from 1- to 3-day-old Sprague-Dawley rat hearts, and adenovirus-mediated gene transfection of NRCMs was performed by methods described previously (*40*). Both NRCMs and NRCFs were cultured in 10% fetal bovine serum (Gibco; Thermo Fisher Scientific Inc., Grand Island, NY, USA) Dulbecco's modified Eagle's medium/F12 medium for 18 hours before their use in subsequent experiments. NRCMs were infected with adenovirus siRNA-control, siRNA-UCHL1, siRNA-siEGFR, Ad-GFP, or Ad-UCHL1 [multiplicity of infection (MOI) = 50].

Adenovirus and adeno-associated virus

Recombinant adenoviruses expressing GFP alone (Ad-GFP), UCHL1 (Ad-UCHL1), siRNA-control, siRNA-UCHL1, or siRNA-EGFR were generated by Hanbio Biotechnology (Shanghai, China). To induce exogenous expression of UCHL1 in vivo, the pAV-CMV-mUCHL1(C-3 × Flag)-P2A-GFP vector (rAAV9-UCHL1) was used (ViGene Biosciences, Shandong, China). Mouse UCHL1 complementary DNA (cDNA) was first amplified by PCR from pCMV6-Entry-mUCHL1 plasmid, and a 3 × Flag-tag was added at the C terminus of UCHL1. The PCR products were digested with Asi SI and Mlu I and inserted into Asi SI Mlu I–digested pAAV9-p2A-GFP to construct the pAV-CMV-mUCHL1 (C-3 × Flag)-P2A-GFP vector (rAAV9-UCHL1). Both UCHL1-Flag and GFP could be expressed in the same cells and tissues and controlled by only one promoter, which was accomplished by using a "self-cleaving" 2A [porcine teschovirus-1 2A (P2A)] sequence (*41*, *42*). AAV carrying GFP (rAAV-GFP) was simultaneously prepared as a control vector. For local knockdown of EGFR in vivo, rAAV9 vectors expressing short hairpin RNAs (shRNA) directed at EGFR (rAAV-siEGFR) or a control hairpin (rAAV-siControl) were used (ViGene Biosciences). The following primer sequences were used: EGFR-siRNA1, 5′-GGAAATTACCTATGTGCAA-3′; EGFR-siRNA2, 5′-AATGGACTTACAGAGCCATCC-3′. The shRNA expression was driven by a mouse U6 promoter (pol III) and used GFP as a reporter. The final virus in normal saline (saline) had a titer of 1×10^{13} to 3.5×10^{13} vg/ml.

Kaplan-Meier curves

The Kaplan-Meier curves for the rAAV9-GFP– and rAAV9-UCHL1–injected mice with or without TAC were produced using GraphPad Prism 5.0 software (GraphPad, San Diego, CA, USA).

Reverse transcription qPCR

Total RNA was isolated from NRCMs and fresh heart tissues using TRIzol reagent (Invitrogen/Thermo Fisher Scientific, Carlsbad, CA, USA) according to the manufacturer's instructions. The first-strand cDNA was synthesized from 1 to 2 μg of total RNA by oligo(dT)-primed RT (iScript cDNA synthesis kit; Bio-Rad Laboratories, Hercules, CA, USA). The mRNA levels of atrial natriuretic peptide (ANP)/ANF, BNP, β-MHC, collagen I, collagen III, and EGFR were determined by real-time qPCR analysis on an Applied Biosystems 7500 Real-Time PCR System using SYBR Green (Applied Biosystems/Thermo Fisher Scientific, Foster City, CA, USA) as described previously (*43*). FAM channel intensity was normalized to ROX intensity, and Ct values were calculated using automatically determined threshold values with SDS software (Applied Biosystems). The levels of detected mRNA were normalized to the amount of endogenous glyceraldehyde-3-phosphate dehydrogenase (GAPDH). The sequences of the qPCR primers are shown in table S2.

Antibodies

The primary and secondary antibodies used in this study are shown as follows and in table S3: anti-Myc (1:2000 dilution), anti-Flag (1:2000 dilution), anti-PGP9.5/UCHL1 (1:800 dilution), anti-GFP (1:5000 dilution), anti-sarcomeric α-actinin (1:200 dilution), anti-EGFR (1:1000 dilution), anti–phospho-EGFR (1:1000 dilution), anti-ubiquitin (1:1000 dilution), anti-AT1/AT1R (1:800 dilution), anti–insulin-like growth factor 1R (IGF1R) (1:1000 dilution), anti-gp130 (1:800 dilution), anti-ErBb2 (1:1000 dilution), anti-ErBb3 (1: 1000 dilution), anti-ErBb4 (1:600 dilution), anti-mouse lgG (1:3000 dilution), anti-rabbit lgG (1:3000 dilution), anti-AKT (1:1000 dilution), anti–phospho-AKT (1:1000 dilution), anti-ERK1/2 (1:2000 dilution), anti–phospho-ERK1/2 (1:1000 dilution), and GAPDH (1:3000 dilution).

Western blot analysis

Cells and heart tissues were lysed with radioimmunoprecipitation assay lysis buffer (Solarbio, Beijing, China). Equal amounts of protein (50 to 60 μg) were separated by SDS–polyacrylamide gel electrophoresis (SDS-PAGE) gels, transferred to polyvinylidene difluoride membranes, and incubated with primary antibodies as indicated for each experiment, followed by incubation with horseradish peroxidase–conjugated secondary antibodies (1:2500) for 1 hour at 20° to 23°C. All blots were developed using a chemiluminescent system, and signal intensities were analyzed with a Gel-Pro 4.5 Analyzer (Media Cybernetics, Rockville, MD, USA).

Immunoprecipitation

NRCMs and HEK293T cells were lysed in lysis buffer [50 mM tris-HCl (pH 8.0), 150 mM NaCl, 0.1% SDS, 1% NP-40, and 0.5% sodium deoxycholate] with PMSF (phenylmethylsulfonyl fluoride) (Solarbio) and protease inhibitor cocktail (Roche, Basel, Switzerland) on ice for 20 min. Lysate was cleared by centrifugation at 12,000 rpm at 4°C for 15 min to obtain the cell extracts. The protein concentration

of the cell extracts was quantitated by bicinchoninic acid (Thermo Fisher Scientific). Immunoprecipitation was performed as described previously (*40*). Briefly, cell extracts were incubated with the appropriate primary antibody (2 μg) and Protein A Sepharose (Amersham Biosciences/GE Healthcare, Chicago, IL, USA) at 4°C for 12 hours, followed by centrifugation at 3000 rpm at 4°C for 10 min. Pellets were washed twice with wash buffer I [50 mM tris-HCl (pH 7.5), 500 mM sodium chloride, 0.1% NP-40, and 0.05% sodium deoxycholate] and once with wash buffer II [50 mM tris-HCl (pH 7.5), 0.1% NP-40, and 0.05% sodium deoxycholate). Bound proteins were eluted by boiling beads in 2 × sample buffer, and the precipitated proteins were subjected to SDS-PAGE using 8 or 10% gels followed by Western blot analysis. Immunoblot data were quantified and analyzed with a Gel-Pro 4.5 Analyzer (Media Cybernetics).

In vivo ubiquitylation assays

To assess endogenous EGFR ubiquitination, NRCMs were infected with adenovirus siRNA-control or siRNA-UCHL1 for 24 hours. To assess ligand-induced EGFR ubiquitination, NRCMs infected with siRNA-control or siRNA-UCHL1 were incubated with EGF (20 ng/ml; Thermo Fisher Scientific, Waltham, MA, USA) and treated with MG132 6 hours before harvest. EGFR was immunoprecipitated with anti-EGFR and detected by Western blot analysis with antibody against Ub. To examine overexpressed EGFR ubiquitylation, HEK293T cells were transfected with expression vectors for GFP-tagged EGFR, Myc-tagged UCHL1 (WT or C90S mutant), or Flag-tagged ubiquitin as indicated in Fig. 4 using Lipofectamine 2000 (Thermo Fisher Scientific). Lysate proteins from cultured cells and heart tissues were precipitated and analyzed by Western blotting using appropriate antibodies (including EGFR, Ub, GFP, Flag, and Myc) as described previously (*40*).

Cardiac hypertrophy models and echocardiography

Male WT and heterozygous UCHL1 knockout (UCHL1$^{+/-}$) mice (8 to 10 weeks of age) were used. Cardiac hypertrophy was induced by TAC for 2 to 6 weeks as described previously (*40*). Animals were lightly anesthetized with isoflurane (1.5%). Cardiac function was evaluated by M-mode and B-mode echocardiography at different time points using a 30-MHz probe (Vevo 770 system; VisualSonics, Toronto, Ontario, Canada). Diastolic and systolic LV wall thickness, LV end-diastolic chamber dimensions, and LV end-systolic chamber dimensions were measured. LV anterior wall at end-diastole (LVAWD), LV anterior wall at end systole (LVAWS), LV internal dimension at end diastole (LVIDD), LV internal dimension at end systole (LVIDS), LV posterior wall at end diastole (LVPWD), and LV posterior wall (LVPWS) at end systole were obtained from original M-mode tracings over three cardiac cycles. The LV EF% and LV FS% were calculated. FS% was calculated using the following formula: %FS = (LVIDD – LVIDD)/(LVIDD).

Histological analysis

The heart size was photographed using a digital camera (Olympus C5060WZ, Japan). The HW, LW, BW, and tibial length (TL) were measured. The LW/TL, HW/BW, and HW/TL ratios were calculated as an index of LV hypertrophy or HF. The heart was fixed in 4% paraformaldehyde solution for 24 hours and then embedded in paraffin. The sections (4 μm) were stained with hematoxylin and eosin (H&E) and Masson's trichrome staining using the standard procedure (*40*, *44*). To assess myocyte size, heart sections were stained with tetramethyl rhodamine isothiocyanate (TRITC)–labeled wheat germ agglutinin [WGA; 50 μg/ml in 1 × phosphate-buffered saline (PBS)] for 1 hour. The cell area was calculated by measuring at least 200 cells per slide. Digital photographs were taken at ×200 magnification of over 20 random fields from each heart and analyzed by Image Pro Plus 3.0 (Nikon, Japan) (*40*).

Immunofluorescence

NRCMs were seeded onto laminin-coated coverslips prior to infection with siRNA-control, siRNA-UCHL1, Ad-GFP, or Ad-UCHL1 for 24 hours, followed by PE stimulation for 24 hours. Immunofluorescence was performed as described previously (*44*). Briefly, the cells were washed with PBS and postfixed in 4% paraformaldehyde for 15 min at 20° to 23°C. After the cells were blocked in PBS containing 1% bovine serum albumin (BSA) and 0.2% Triton X-100 for 10 min, monoclonal antibody against sarcomeric α-actinin was added at dilutions of 1:200 for overnight incubation at 4°C. After washing with PBS three times for 5 min, the cells were then incubated with secondary antibody for 1 hour at 20° to 23°C, and the nuclear staining was performed with 4′,6-diamidino-2-phenylindole (DAPI; 100 ng/ml) for 5 min. The cardiomyocyte surface area was depicted using ImageJ software (NIH, Bethesda, MD, USA), and the relative surface area was read with arbitrary units (the number of pixels) to evaluate hypertrophy.

TUNEL assay

Apoptosis of heart sections and cardiomyocytes was detected using an In Situ Cell Death Detection Kit (TUNEL fluorescence FITC kit; Roche, Indianapolis, IN, USA) according to the manufacturer's instructions. The heart sections were stained with a commercially available TUNEL kit. Nuclei were counterstained with DAPI (Sigma-Aldrich, St. Louis, MO, USA). To identify cardiomyocytes, counterstaining by primary antibody a-actinin (Sigma-Aldrich) was performed after TUNEL staining. Fluorescence staining was viewed by microscopy (Nikon). Six to eight visual fields were randomly selected from each section. The percentage of TUNEL-positive nuclei was calculated as the sum of all double-positive nuclei divided by the sum of all nuclei.

Immunohistochemistry analysis of human hearts

The study included three male patients and three age- and gender-matched controls. Samples from patients with HF were obtained from Beijing Anzhen Hospital of the Capital University of Medical Sciences at the time of cardiac transplantation. Normal hearts (non-failing hearts as controls) were obtained from donors with normal cardiac contractile function based on echocardiography of those who had died from motor vehicle accidents. The three male donors had a median age of 48 years. The three HF patients (male) had a median age of 46 years, and their average EF% was 20 ± 5%. The study was performed in accordance with the Declaration of Helsinki and approved by the Institutional Review Board of Beijing Anzhen Hospital, Capital Medical University. Patients provided written consent. Heart tissues were fixed in neutral buffered formalin solution, embedded in paraffin, and then cut into 5-μm serial sections. Immunohistochemistry staining was performed as described previously (*44*). Monoclonal antibody UCHL1 (1:100 dilution) and BNP (1:100 dilution) were used as primary antibodies.

LDN-57444 administration

Male WT mice were randomly subjected to sham or TAC operation for 2 weeks and then intraperitoneal administration with UCHL1

inhibitor LDN-57444 (40 μg/kg, one time per day) or vehicle. Sham-operated animals underwent the identical surgical procedure except that the ligature was not tied. The hearts were removed for further analysis.

Microarray assay

Microarray was performed as previously described, and the details of our gene expression data are available at the GEO website www.ncbi.nlm.nih.gov/geo/ (accession number GSE59437) (*12*).

Statistical analysis

Statistical calculations were performed using SPSS version 16.0 (SPSS Inc., Chicago, IL, USA). Sample numbers are shown in the figures and figure legends and in Materials and Methods. First, the normality test was performed. If each group satisfied the normality and the variance between the groups was equal, we used Student's *t* test to determine the significant difference between two groups, and one-way analysis of variance (ANOVA) with the Bonferroni post hoc test for comparisons among more than two groups; if the above conditions were not met, we used the nonparametric Mann-Whitney *U* test. Statistical differences in means were considered statistically significant at $P < 0.05$.

SUPPLEMENTARY MATERIALS

Supplementary material for this article is available at http://advances.sciencemag.org/cgi/content/full/6/16/eaax4826/DC1

View/request a protocol for this paper from *Bio-protocol*.

REFERENCES AND NOTES

1. J. Heineke, J. D. Molkentin, Regulation of cardiac hypertrophy by intracellular signalling pathways. *Nat. Rev. Mol. Cell Biol.* **7**, 589–600 (2006).
2. M. A. de Korte, E. G. de Vries, M. N. Lub-de Hooge, P. L. Jager, J. A. Gietema, W. T. van der Graaf, W. J. Sluiter, D. J. van Veldhuisen, T. M. Suter, D. T. Sleijfer, P. J. Perik, 111Indium-trastuzumab visualises myocardial human epidermal growth factor receptor 2 expression shortly after anthracycline treatment but not during heart failure: A clue to uncover the mechanisms of trastuzumab-related cardiotoxicity. *Eur. J. Cancer* **43**, 2046–2051 (2007).
3. Y. Yarden, G. Pines, The ERBB network: At last, cancer therapy meets systems biology. *Nat. Rev. Cancer* **12**, 553–563 (2012).
4. N. Makki, K. W. Thiel, F. J. Miller Jr., The epidermal growth factor receptor and its ligands in cardiovascular disease. *Int. J. Mol. Sci.* **14**, 20597–20613 (2013).
5. Y. L. Deribe, P. Wild, A. Chandrashaker, J. Curak, M. H. H. Schmidt, Y. Kalaidzidis, N. Milutinovic, I. Kratchmarova, L. Buerkle, M. J. Fetchko, P. Schmidt, S. Kittanakom, K. R. Brown, I. Jurisica, B. Blagoev, M. Zerial, I. Stagljar, I. Dikic, Regulation of epidermal growth factor receptor trafficking by lysine deacetylase HDAC6. *Sci. Signal.* **2**, ra84 (2009).
6. W. R. Critchley, C. Pellet-Many, B. Ringham-Terry, M. A. Harrison, I. C. Zachary, S. Ponnambalam, Receptor tyrosine kinase ubiquitination and de-ubiquitination in signal transduction and receptor trafficking. *Cell* **7**, E22 (2018).
7. Y. Goto, L. Zeng, C. J. Yeom, Y. Zhu, A. Morinibu, K. Shinomiya, M. Kobayashi, K. Hirota, S. Itasaka, M. Yoshimura, K. Tanimoto, M. Torii, T. Sowa, T. Menju, M. Sonobe, H. Kakeya, M. Toi, H. Date, E. M. Hammond, M. Hiraoka, H. Harada, UCHL1 provides diagnostic and antimetastatic strategies due to its deubiquitinating effect on HIF-1α. *Nat. Commun.* **6**, 6153 (2015).
8. J. Choi, A. I. Levey, S. T. Weintraub, H. D. Rees, M. Gearing, L. S. Chin, L. Li, Oxidative modifications and down-regulation of ubiquitin carboxyl-terminal hydrolase L1 associated with idiopathic Parkinson's and Alzheimer's diseases. *J. Biol. Chem.* **279**, 13256–13264 (2004).
9. C. L. Wilson, L. B. Murphy, J. Leslie, S. Kendrick, J. French, C. R. Fox, N. S. Sheerin, A. Fisher, J. H. Robinson, D. G. Tiniakos, D. A. Gray, F. Oakley, D. A. Mann, Ubiquitin C-terminal hydrolase 1: A novel functional marker for liver myofibroblasts and a therapeutic target in chronic liver disease. *J. Hepatol.* **63**, 1421–1428 (2015).
10. K. Yamazaki, N. Wakasugi, T. Tomita, T. Kikuchi, M. Mukoyama, K. Ando, Gracile axonal dystrophy (GAD), a new neurological mutant in the mouse. *Proc. Soc. Exp. Biol. Med.* **187**, 209–215 (1988).
11. A. Drobysheva, M. Ahmad, R. White, H. W. Wang, F. H. Leenen, Cardiac sympathetic innervation and PGP9.5 expression by cardiomyocytes after myocardial infarction: Effects of central MR blockade. *Am. J. Physiol. Heart Circ. Physiol.* **305**, H1817–H1829 (2013).
12. M. Q. Dang, X. C. Zhao, S. Lai, X. Wang, L. Wang, Y.-L. Zhang, Y. Liu, X.-H. Yu, Y. Liu, H.-H. Li, Y.-L. Xia, Gene expression profile in the early stage of angiotensin II-induced cardiac remodeling: A time series microarray study in a mouse model. *Cell. Physiol. Biochem.* **35**, 467–476 (2015).
13. E. Y. Seo, S. P. Jin, K. C. Sohn, C. H. Park, D. H. Lee, J. H. Chung, UCHL1 regulates melanogenesis through controlling MITF stability in human melanocytes. *J. Invest. Dermatol.* **137**, 1757–1765 (2017).
14. Y. Liu, L. Fallon, H. A. Lashuel, Z. Liu, P. T. Lansbury Jr., The UCH-L1 gene encodes two opposing enzymatic activities that affect alpha-synuclein degradation and Parkinson's disease susceptibility. *Cell* **111**, 209–218 (2002).
15. M. Sibilia, E. F. Wagner, Strain-dependent epithelial defects in mice lacking the EGF receptor. *Science* **269**, 234–238 (1995).
16. E. Kobayashi, M. Aga, S. Kondo, C. Whitehurst, T. Yoshizaki, J. S. Pagano, J. Shackelford, C-terminal farnesylation of UCH-L1 plays a role in transport of Epstein-Barr virus primary oncoprotein LMP1 to exosomes. *mSphere* **3**, e00030-18 (2018).
17. Y. Liu, H. A. Lashuel, S. Choi, X. Xing, A. Case, J. Ni, L. A. Yeh, G. D. Cuny, R. L. Stein, P. T. Lansbury Jr., Discovery of inhibitors that elucidate the role of UCH-L1 activity in the H1299 lung cancer cell line. *Chem. Biol.* **10**, 837–846 (2003).
18. Y. Y. Gu, M. Yang, M. Zhao, Q. Luo, L. Yang, H. Peng, J. Wang, S. K. Huang, Z. X. Zheng, X. H. Yuan, P. Liu, C. Z. Huang, The de-ubiquitinase UCHL1 promotes gastric cancer metastasis via the Akt and Erk1/2 pathways. *Tumour Biol.* **36**, 8379–8387 (2015).
19. M. Zhang, Y. Deng, Y. Luo, S. Zhang, H. Zou, F. Cai, K. Wada, W. Song, Control of BACE1 degradation and APP processing by ubiquitin carboxyl-terminal hydrolase L1. *J. Neurochem.* **120**, 1129–1138 (2012).
20. M. Zhang, F. Cai, S. Zhang, S. Zhang, W. Song, Overexpression of ubiquitin carboxyl-terminal hydrolase L1 (UCHL1) delays Alzheimer's progression in vivo. *Sci. Rep.* **4**, 7298 (2014).
21. H. F. Nural-Guvener, N. Mutlu, M. A. Gaballa, BACE1 levels are elevated in congestive heart failure. *Neurosci. Lett.* **532**, 7–11 (2013).
22. J. Li, J. Zeng, L. Wu, L. Tao, Z. Liao, M. Chu, L. Li, Loss of P53 regresses cardiac remodeling induced by pressure overload partially through inhibiting HIF1α signaling in mice. *Biochem. Biophys. Res. Commun.* **501**, 394–399 (2018).
23. D. Xu, R. Liao, X. X. Wang, Z. Cheng, Effects of miR-155 on hypertensive rats via regulating vascular mesangial hyperplasia. *Eur. Rev. Med. Pharmacol. Sci.* **22**, 7431–7438 (2018).
24. S. Usui, Y. Maejima, J. Pain, C. Hong, J. Cho, J. Y. Park, D. Zablocki, B. Tian, D. J. Glass, J. Sadoshima, Endogenous muscle atrophy F-box mediates pressure overload-induced cardiac hypertrophy through regulation of nuclear factor-kappaB. *Circ. Res.* **109**, 161–171 (2011).
25. C. L. Galindo, M. A. Skinner, M. Errami, L. D. Olson, D. A. Watson, J. Li, J. F. McCormick, L. J. McIver, N. M. Kumar, T. Q. Pham, H. R. Garner, Transcriptional profile of isoproterenol-induced cardiomyopathy and comparison to exercise-induced cardiac hypertrophy and human cardiac failure. *BMC Physiol.* **9**, 23 (2009).
26. S. M. Yu, P. Y. Jean-Charles, D. M. Abraham, S. Kaur, C. Gareri, L. Mao, H. A. Rockman, S. K. Shenoy, The deubiquitinase ubiquitin-specific protease 20 is a positive modulator of myocardial β_1-adrenergic receptor expression and signaling. *J. Biol. Chem.* **294**, 2500–2518 (2019).
27. T. K. Sin, B. T. Tam, B. Y. Yung, S. P. Yip, L. W. Chan, C. S. Wong, M. Ying, J. A. Rudd, P. M. Siu, Resveratrol protects against doxorubicin-induced cardiotoxicity in aged hearts through the SIRT1-USP7 axis. *J. Physiol.* **593**, 1887–1899 (2015).
28. H. Wang, Y. Lai, B. J. Mathis, W. Wang, S. Li, C. Qu, B. Li, L. Shao, H. Song, J. S. Janicki, S. C. Sun, X. L. Wang, D. Tang, T. Cui, Deubiquitinating enzyme CYLD mediates pressure overload-induced cardiac maladaptive remodeling and dysfunction via downregulating Nrf2. *J. Mol. Cell. Cardiol.* **84**, 143–153 (2015).
29. S. Packham, Y. Lin, Z. Zhao, D. Warsito, D. Rutishauser, O. Larsson, The nucleus-localized epidermal growth factor receptor is SUMOylated. *Biochemistry* **54**, 5157–5166 (2015).
30. T. Wang, J. Yang, J. Xu, J. Li, Z. Cao, L. Zhou, L. You, H. Shu, Z. Lu, H. Li, M. Li, T. Zhang, Y. Zhao, CHIP is a novel tumor suppressor in pancreatic cancer through targeting EGFR. *Oncotarget* **5**, 1969–1986 (2014).
31. F. Huang, D. Kirkpatrick, X. Jiang, S. Gygi, A. Sorkin, Differential regulation of EGF receptor internalization and degradation by multiubiquitination within the kinase domain. *Mol. Cell* **21**, 737–748 (2006).
32. J. McCullough, M. J. Clague, S. Urbé, AMSH is an endosome-associated ubiquitin isopeptidase. *J. Cell Biol.* **166**, 487–492 (2004).
33. F. Pareja, D. A. Ferraro, C. Rubin, H. Cohen-Dvashi, F. Zhang, S. Aulmann, N. Ben-Chetrit, G. Pines, R. Navon, N. Crosetto, W. Kostler, S. Carvalho, S. Lavi, F. Schmitt, I. Dikic, Z. Yakhini, P. Sinn, G. B. Mills, Y. Yarden, Deubiquitination of EGFR by Cezanne-1 contributes to cancer progression. *Oncogene* **31**, 4599–4608 (2012).
34. K. K. Guturi, T. Mandal, A. Chatterjee, M. Sarkar, S. Bhattacharya, U. Chatterjee, M. K. Ghosh, Mechanism of β-catenin-mediated transcriptional regulation of epidermal

growth factor receptor expression in glycogen synthase kinase 3 β-inactivated prostate cancer cells. *J. Biol. Chem.* **287**, 18287–18296 (2012).
35. S. C. Peng, Y. T. Lai, H. Y. Huang, H. D. Huang, Y. S. Huang, A novel role of CPEB3 in regulating EGFR gene transcription via association with Stat5b in neurons. *Nucleic Acids Res.* **38**, 7446–7457 (2010).
36. J. Cai, L. Xu, Z. Cai, J. Wang, B. Zhou, H. Hu, MicroRNA-146b-5p inhibits the growth of gallbladder carcinoma by targeting epidermal growth factor receptor. *Mol. Med. Rep.* **12**, 1549–1555 (2015).
37. H. Ohtsu, G. D. Frank, H. Utsunomiya, S. Eguchi, Redox-dependent protein kinase regulation by angiotensin II: Mechanistic insights and its pathophysiology. *Antioxid. Redox Signal.* **7**, 1315–1326 (2005).
38. P. O. Hackel, E. Zwick, N. Prenzel, A. Ullrich, Epidermal growth factor receptors: Critical mediators of multiple receptor pathways. *Curr. Opin. Cell Biol.* **11**, 184–189 (1999).
39. H. J. Kim, Y. M. Kim, S. Lim, Y. K. Nam, J. Jeong, H. J. Kim, K. J. Lee, Ubiquitin C-terminal hydrolase-L1 is a key regulator of tumor cell invasion and metastasis. *Oncogene* **28**, 117–127 (2009).
40. H.-H. Li, V. Kedar, C. Zhang, H. McDonough, R. Arya, D.-Z. Wang, C. Patterson, Atrogin-1/muscle atrophy F-box inhibits calcineurin-dependent cardiac hypertrophy by participating in an SCF ubiquitin ligase complex. *J. Clin. Invest.* **114**, 1058–1071 (2004).
41. Z. Liu, O. Chen, J. B. J. Wall, M. Zheng, Y. Zhou, L. Wang, H. Ruth Vaseghi, L. Qian, J. Liu, Systematic comparison of 2A peptides for cloning multi-genes in a polycistronic vector. *Sci. Rep.* **7**, 2193 (2017).
42. J. H. Kim, S. R. Lee, L. H. Li, H. J. Park, J. H. Park, K. Y. Lee, M. K. Kim, B. A. Shin, S. Y. Choi, High cleavage efficiency of a 2A peptide derived from porcine teschovirus-1 in human cell lines, zebrafish and mice. *PLOS ONE* **6**, e18556 (2011).
43. H.-H. Li, M. S. Willis, P. Lockyer, N. Miller, H. McDonough, D. J. Glass, C. Patterson, Atrogin-1 inhibits Akt-dependent cardiac hypertrophy in mice via ubiquitin-dependent coactivation of Forkhead proteins. *J. Clin. Invest.* **117**, 3211–3223 (2007).
44. X. Xie, H.-L. Bi, S. Lai, Y.-L. Zhang, N. Li, H.-J. Cao, L. Han, H.-X. Wang, H.-H. Li, The immunoproteasome catalytic β5i subunit regulates cardiac hypertrophy by targeting the autophagy protein ATG5 for degradation. *Sci. Adv.* **5**, eaau0495 (2019).

Acknowledgments: We would like to thank J. Wang and Y. Zhang for helping with mouse colony management and assistance with animal procedures and experiments. **Funding:** This work was supported by grants from the National Natural Science Foundation of China (31571170, 81330003, and 81630009 to H.-H.L.; 81700350 to H.-L.B.), Dalian High-level Talents Innovation and Entrepreneurship Projects (2015R019), and the Chang Jiang Scholar Program of China (T2011160, to H.-H.L). **Author contributions:** H.-H.L. conceived the project. H.-L.B. and X.-L.Z. performed and analyzed in vivo experiments. H.-L.B. and Y.-L.Z. performed the in vitro experiments and analyzed the data. X.X. performed and analyzed the biochemical and biophysical experiments. J.D. and Y.-L.X. were responsible for human clinical and molecular genetic studies. H.-H.L. and H.-L.B. wrote the paper with input from all authors. The images were photographed by H.-L.B., Department of Cardiology, First Affiliated Hospital of Dalian Medical University. **Competing interests:** The authors declare that they have no competing interests. **Data and materials availability:** All data needed to evaluate the conclusions of the paper are present in the paper and/or the Supplementary Materials. Additional data related to this paper may be requested from the authors.

Submitted 19 April 2019
Accepted 23 January 2020
Published 17 April 2020
10.1126/sciadv.aax4826

Citation: H.-L. Bi, X.-L. Zhang, Y.-L. Zhang, X. Xie, Y.-L. Xia, J. Du, H.-H. Li, The deubiquitinase UCHL1 regulates cardiac hypertrophy by stabilizing epidermal growth factor receptor. *Sci. Adv.* **6**, eaax4826 (2020).

The deubiquitinase UCHL1 regulates cardiac hypertrophy by stabilizing epidermal growth factor receptor

Hai-Lian Bi, Xiao-Li Zhang, Yun-Long Zhang, Xin Xie, Yun-Long Xia, Jie Du and Hui-Hua Li

Sci Adv **6** (16), eaax4826.
DOI: 10.1126/sciadv.aax4826